An Asymptotic-Preserving method for highly anisotropic elliptic equations based on a micro-macro decomposition

Pierre Degond[†‡] Alexei Lozinski[†] Jacek Narski[†] Claudia Negulescu[§]

February 4, 2011

Abstract

The concern of the present work is the introduction of a very efficient Asymptotic Preserving scheme for the resolution of highly anisotropic diffusion equations. The characteristic features of this scheme are the uniform convergence with respect to the anisotropy parameter $0 < \varepsilon << 1$, the applicability (on cartesian grids) to cases of non-uniform and non-aligned anisotropy fields b and the simple extension to the case of a non-constant anisotropy intensity $1/\varepsilon$. The mathematical approach and the numerical scheme are different from those presented in the previous work [Degond et al. (2010), arXiv:1008.3405v1] and its considerable advantages are pointed out.

1 Introduction

The numerical resolution of highly anisotropic physical problems is a challenging task. In particular, it is difficult to capture the behaviour of physical phenomena characterized by strong anisotropic features since a straight-forward discretization leads typically to very ill-conditioned problems. In the class of problems addressed in this paper the anisotropy is aligned with a vector field which may be variable in space/time. Such problems are encountered in many physical applications, for example flows in porous media [3, 10], semiconductor modeling [14], quasi-neutral plasma simulations [7], the list of possible applications being not exhaustive. The motivation of this work is closely related to the magnetized plasma simulations such as atmospheric plasmas [12, 13], internal fusion plasmas [4, 9] or plasma thrusters [1]. In this case the anisotropy direction is defined by a magnetic field confining the particles around the field lines, the anisotropy intensity $1/\varepsilon$ reaching orders of magnitude as high as 10^{10}. The difficulty with these anisotropic problems is that they become singular in the limit $\varepsilon \to 0$, where ε is a small parameter responsible for the strong anisotropy of the problem. A straightforward discretization of such problems (using, for example, finite difference methods) results in the inversion of a very badly conditioned linear system, which becomes unfeasible for $\varepsilon << 1$. In this paper we present a new approach based on the so called Asymptotic Preserving reformulation introduced initially in [11]. This work presents an important improvement to the method presented in the previous paper [6] and is aimed to treat in a precise manner a variety of strong anisotropies with low numerical costs.

[†]Université de Toulouse, UPS, INSA, UT1, UTM, Institut de Mathématiques de Toulouse, F-31062 Toulouse, France
[‡]CNRS, Institut de Mathématiques de Toulouse UMR 5219, F-31062 Toulouse, France
[§]CMI/LATP, Université de Provence, 39 rue Frédéric Joliot-Curie 13453 Marseille cedex 13

The model problem we are interested in, reads

$$\begin{cases} -\nabla \cdot \mathbb{A}\nabla u^\varepsilon = f & \text{in } \Omega, \\ n \cdot \mathbb{A}\nabla u^\varepsilon = 0 & \text{on } \Gamma_N\,, \\ u^\varepsilon = 0 & \text{on } \Gamma_D\,, \end{cases} \tag{1}$$

where $\Omega \subset \mathbb{R}^2$ or $\Omega \subset \mathbb{R}^3$ is a bounded domain with boundary $\partial\Omega = \Gamma_D \cup \Gamma_N$ and outward normal n. The direction of the anisotropy is given by a vector field B, where we suppose $\mathrm{div} B = 0$ and $B \neq 0$. The direction of B shall be denoted by the unit vector field $b = B/|B|$. The domain boundary is decomposed into $\Gamma_D := \{x \in \partial\Omega \mid b(x) \cdot n = 0\}$ and $\Gamma_N := \partial\Omega \backslash \Gamma_D$. The anisotropic diffusion matrix is then given by

$$\mathbb{A} = \frac{1}{\varepsilon} A_\parallel b \otimes b + (Id - b \otimes b) A_\perp (Id - b \otimes b)\,. \tag{2}$$

The scalar field $A_\parallel > 0$ and the symmetric positive definite matrix field $A_\perp$ are of order one while the parameter $0 < \varepsilon < 1$ can be very small, provoking thus the high anisotropy of the problem. The system becomes ill posed if we consider the formal limit $\varepsilon \to 0$. It is thus very ill conditioned for $\varepsilon << 1$. The goal of the present paper is to circumvent this difficulty and to propose a numerical scheme which is uniformly convergent with respect to the parameter ε.

This model problem has been studied before in the Asymptotic Preserving context, see for example [8, 5, 6]. The key idea was to decompose the solution u^ε into two parts: p^ε, which is constant along the anisotropy direction and q^ε, which contains the fluctuating part. The resulting modified linear system is bigger than the original problem but has the important feature of reducing, as $\varepsilon \to 0$, to the so-called *Limit* model (L-model), which is a well-posed system satisfied by the limit solution $u^0 = \lim_{\varepsilon \to 0} u^\varepsilon$. In other words, this AP-procedure transforms a singularly perturbed problem in an equivalent regularly perturbed one.

In [8], a special case of an anisotropy aligned with the z-axis was studied. The Asymptotic Preserving reformulation was obtained in the following way. Firstly, the original problem was integrated along the anisotropy direction, resulting in an ε-independent elliptic equation for the mean part p^ε. Then, the mean equation was subtracted from the original problem giving rise to an elliptic equation for the fluctuating part q^ε. A generalization of this approach was proposed in [5], in the framework of curvilinear anisotropy fields b. The introduction of an adapted curvilinear coordinate system with one coordinate aligned with the anisotropy direction allowed to reduce the problem to the one studied in [8] and hence to address more realistic problems, as for example the ionospheric plasma simulations.

In [6], the original method of [8] is generalized for arbitrary fields b in a different manner. Instead of performing a coordinate-system transformation and integrating along the anisotropy direction, the new technique uses a Cartesian grid in combination with an adapted mathematical framework. The mean part p^ε is forced to be in the space of functions constant along the b field by means of a Lagrange multiplier technique. Similarly, the fluctuating part q^ε is forced to be in the orthogonal space (with respect to the L^2-norm). This approach requires the introduction of three Lagrange multipliers and results in a system with five unknowns. The advantage of this method lies in its generality. Since no change of the coordinate system is needed, no computation of the field lines, no integration along them as well as no mesh adaptation is required, this numerical method is easy to implement even for anisotropies varying in time. The method works well on Cartesian grids even for strongly varying b fields. We will refer to the method of [6] as the Duality-Based (DB) Asymptotic Preserving reformulation or simply as the DB-method, to emphasize the extensive use of Lagrange multipliers in its derivation.

In the present paper we introduce a novel approach. It is as general as the DB-method, i.e. no change of coordinate system nor mesh adaptation is required. It is however much more efficient in terms of computational cost. The new idea arises from the following questions: does p^ε need to be the average of u^ε along the anisotropy direction? Does q^ε need to be orthogonal to p^ε, with respect to the L^2-norm? Is $u^\varepsilon = p^\varepsilon + q^\varepsilon$ an optimal decomposition? In this paper we exploit a different decomposition: $u^\varepsilon = p^\varepsilon + \varepsilon q^\varepsilon$, with q^ε not being orthogonal to p^ε. Instead, q^ε belongs to the space of functions vanishing on the "inflow" part of the boundary, i.e. where $b \cdot n < 0$. This space is easy to discretize without introducing any additional Lagrange multiplier. As a result, p^ε is no longer an average of u^ε, however we still choose it to be constant along the anisotropy direction. The AP reformulation of the original equation is then obtained in terms of u^ε and q^ε. We use first the fact that the only component of u^ε that varies along the anisotropy direction is $\varepsilon q^\varepsilon$, and thus replace $\nabla_{||} u^\varepsilon$ by $\varepsilon \nabla_{||} q^\varepsilon$ in the term of order $1/\varepsilon$. We obtain thus an equation whose coefficients are all of order one. We should add also a second equation assuring than $p^\varepsilon = u^\varepsilon - \varepsilon q^\varepsilon$ is indeed constant along the field lines. The resulting system consists of only two equations compared to the five equations of the DB-method. It should be noted that, while keeping the advantages of the DB-method (no need of mesh- or coordinate-system-adaptation with respect to the anisotropy direction, uniform convergence with respect to ε), the new method is far more efficient in terms of memory requirements as well as computational time. The new method will be referred to as the Micro-Macro (MM) Asymptotic Preserving reformulation or simply as the MM-method, to emphasize the fact that the fluctuating part q^ε of the solution is now rescaled by ε. We will prove, in particular, that q^ε does not explode as $\varepsilon \to 0$, so that the ansatz $u^\varepsilon = p^\varepsilon + \varepsilon q^\varepsilon$ does indeed introduce a proper rescaling for the "micro"-fluctuations over the "macro" part of the solution contained in p^ε.

The paper is organized as follows. Section 2 introduces the Singularly Perturbed elliptic problem (P-model) and the new Asymptotic Preserving reformulation (MM-method). We also perform a mathematical study of this reformulation, in particular, of the convergence towards the Limit model, as $\varepsilon \to 0$. In Section 3 we present the discretization and the numerical results of various test cases for constant and variable anisotropy fields b. We compare the efficiency of the new MM-method with the previously proposed DB-method. Finally, in Section 4 we propose a generalization of the MM-method to the case of a non-constant anisotropy parameter ε. The detailed numerical analysis of the MM-method is postponed to a forthcoming work.

2 The mathematical problem

Let b be a smooth field in a domain $\Omega \subset \mathbb{R}^d$, with $d = 2, 3$, and let us decompose the boundary $\Gamma = \partial\Omega$ into three components following the sign of the intersection with b:

$$\Gamma_D := \{x \in \Gamma \ / \ b(x) \cdot n(x) = 0\}\,, \quad \Gamma_{in} := \{x \in \Gamma \ / \ b(x) \cdot n(x) < 0\}\,, \quad \Gamma_{out} := \{x \in \Gamma \ / \ b(x) \cdot n(x) > 0\}\,.$$

The vector n is here the unit outward normal on Γ. We denote $\Gamma_N := \Gamma_{in} \cup \Gamma_{out}$. We also assume $b \in (C^\infty(\bar{\Omega}))^d$ and $|b(x)| = 1$ for all $x \in \bar{\Omega}$.

Given this vector field b, one can decompose now vectors $v \in \mathbb{R}^d$, gradients $\nabla\phi$, with $\phi(x)$ a scalar function, and divergences $\nabla \cdot v$, with $v(x)$ a vector field, into a part parallel to the anisotropy direction and a part perpendicular to it. These parts are defined as follows:

$$\begin{aligned}
&v_{||} := (v \cdot b)b\,, && v_\perp := (Id - b \otimes b)v\,, && \text{such that} \quad v = v_{||} + v_\perp\,,\\
&\nabla_{||}\phi := (b \cdot \nabla\phi)b\,, && \nabla_\perp\phi := (Id - b \otimes b)\nabla\phi\,, && \text{such that} \quad \nabla\phi = \nabla_{||}\phi + \nabla_\perp\phi\,,\\
&\nabla_{||} \cdot v := \nabla \cdot v_{||}\,, && \nabla_\perp \cdot v := \nabla \cdot v_\perp\,, && \text{such that} \quad \nabla \cdot v = \nabla_{||} \cdot v + \nabla_\perp \cdot v\,,
\end{aligned} \tag{3}$$

where we denoted by $\otimes$ the vector tensor product. With these notations we can now introduce the mathematical problem, the so-called Singular Perturbation problem, whose numerical solution is the main concern of this paper.

2.1 The Singular-Perturbation problem (P-model)

Our starting problem is the following Singular-Perturbation problem (P-problem)

$$(P)\quad \begin{cases} -\frac{1}{\varepsilon}\nabla_{\|}\cdot\left(A_{\|}\nabla_{\|}u^{\varepsilon}\right)-\nabla_{\perp}\cdot\left(A_{\perp}\nabla_{\perp}u^{\varepsilon}\right)=f & \text{in } \Omega,\\ \frac{1}{\varepsilon}n_{\|}\cdot\left(A_{\|}\nabla_{\|}u^{\varepsilon}\right)+n_{\perp}\cdot\left(A_{\perp}\nabla_{\perp}u^{\varepsilon}\right)=0 & \text{on } \Gamma_N,\\ u^{\varepsilon}=0 & \text{on } \Gamma_D\,. \end{cases} \tag{4}$$

The diffusion coefficients and the source term satisfy

Hypothesis A *Let $f\in L^2(\Omega)$, $0<\varepsilon<1$ be a fixed arbitrary parameter and $\overset{\circ}{\Gamma}_D\neq\varnothing$. The diffusion coefficients $A_{||}\in L^{\infty}(\Omega)$ and $A_{\perp}\in\mathbb{M}_{d\times d}(L^{\infty}(\Omega))$ are supposed to satisfy*

$$0<A_0\leq A_{||}(x)\leq A_1\,,\quad f.a.a\ x\in\Omega, \tag{5}$$

$$A_0||v||^2\leq v^tA_{\perp}(x)v\leq A_1||v||^2\,,\quad \forall v\in\mathbb{R}^d\ \text{ with }\ v\cdot b(x)=0\ \text{ and }\ f.a.a\ x\in\Omega, \tag{6}$$

with some constants $0<A_0\leq A_1$.

For the beginning we shall consider a constant anisotropy intensity ε (no space dependence) in order to better understand and study the construction of the AP-reformulation. Later on, in section 4 we shall generalize the AP-reformulation to variable ε cases.

As we intend to use the finite element method for the numerical solution of the P-problem, let us put (4) under variational form. For this, let us introduce the Hilbert-space

$$\mathcal{V}=\{v\in H^1(\Omega)\,,\ \text{such that } v|_{\Gamma_D}=0\}\,,\quad (u,v)_{\mathcal{V}}:=(\nabla_{||}u,\nabla_{||}v)+(\nabla_{\perp}u,\nabla_{\perp}v)\,, \tag{7}$$

and its subspace

$$\mathcal{G}=\{v\in\mathcal{V}\,,\ \text{such that } \nabla_{||}v=0\}\,,\quad (u,v)_{\mathcal{G}}:=(\nabla_{\perp}u,\nabla_{\perp}v)\,, \tag{8}$$

where $(\cdot,\cdot)$ shall stand in the following for the standard L^2-scalar product.

We are seeking thus for $u^{\varepsilon}\in\mathcal{V}$, solution of

$$(P)\qquad a_{||}(u^{\varepsilon},v)+\varepsilon a_{\perp}(u^{\varepsilon},v)=\varepsilon(f,v)\,,\quad \forall v\in\mathcal{V}\,, \tag{9}$$

where the continuous bilinear forms $a_{||}:\mathcal{V}\times\mathcal{V}\to\mathbb{R}$ and $a_{\perp}:\mathcal{V}\times\mathcal{V}\to\mathbb{R}$ are given by

$$a_{||}(u,v)\ :=\ \int_{\Omega}A_{||}\nabla_{||}u\cdot\nabla_{||}v\,dx\,,\quad a_{\perp}(u,v):=\int_{\Omega}(A_{\perp}\nabla_{\perp}u)\cdot\nabla_{\perp}v\,dx\,. \tag{10}$$

Thanks to Hypothesis A and to the Lax-Milgram theorem, problem (9) admits a unique solution $u^{\varepsilon}\in\mathcal{V}$ for all fixed $\varepsilon>0$. The parameter $0<\varepsilon<1$ is responsible for the high anisotropy of the problem, and its smallness induces severe numerical difficulties. Indeed, putting formally $\varepsilon=0$ in (9), yields $a_{||}(u^0,v)=0$ for all $v\in\mathcal{V}$, which has infinitely many solutions, constant along the field lines. We see thus that the system (9) becomes degenerate in the limit $\varepsilon\to0$. It means that solving (9) for $0<\varepsilon<<1$ with standard numerical schemes is very inadequate, since we have to deal with very ill-conditioned linear systems.

However, as detailed in [6], the solution $u^\varepsilon \in \mathcal{V}$ of (4) is shown to tend as $\varepsilon \to 0$ towards a function $u^0 \in \mathcal{G}$, constant along the field lines of b and solution of the Limit model

$$(L) \qquad \int_\Omega (A_\perp \nabla_\perp u^0) \cdot \nabla_\perp v \, dx = \int_\Omega f v \, dx \,, \quad \forall v \in \mathcal{G} \,. \tag{11}$$

Again, the Lax-Milgram theorem permits to show the existence and uniqueness of a solution $u^0 \in \mathcal{G}$ of this Limit problem (11).

The aim of the present work, is to introduce an AP-scheme (Asymptotic Preserving), which shall permit to find numerically the solution of problem (4) (or (9) equivalently) in an accurate manner, independently on ε and with only moderate requirements concerning computer resources. This shall be based on the introduction of an equivalent reformulation of the P-model, which shall permit to pass continuously from the reformulated P-model (9) to the L-model (11) as $\varepsilon \to 0$. In other words, this reformulation of the P-model will simply be a regular perturbation of the L-model, avoiding thus the encountered problems of ill-posedness, when passing to the limit directly in the singularly perturbed problem (9). This procedure leads to some considerable numerical advantages for $0 < \varepsilon << 1$.

2.2 An AP- reformulation of the problem (MM-problem)

To introduce a reformulation of the P-model, which shall be well-posed in the limit $\varepsilon \to 0$, we need the following Hilbert space

$$\mathcal{L} = \{q \in L^2(\Omega) \ / \ \nabla_{||} q \in L^2(\Omega) \text{ and } q|_{\Gamma_{in}} = 0\} \,, \quad (q,w)_{\mathcal{L}} := (\nabla_{||} q, \nabla_{||} w) \,, \quad \forall q, w \in \mathcal{L} \,. \tag{12}$$

Consider the following problem, called in the sequel Asymptotic-Preserving problem based on a micro-macro decompostion (MM-problem): find $(u^\varepsilon, q^\varepsilon) \in \mathcal{V} \times \mathcal{L}$, solution of

$$(MM) \quad \begin{cases} \displaystyle\int_\Omega (A_\perp \nabla_\perp u^\varepsilon) \cdot \nabla_\perp v \, dx + \int_\Omega A_{||} \nabla_{||} q^\varepsilon \cdot \nabla_{||} v \, dx = \int_\Omega f v \, dx, & \forall v \in \mathcal{V} \\ \displaystyle\int_\Omega A_{||} \nabla_{||} u^\varepsilon \cdot \nabla_{||} w \, dx - \varepsilon \int_\Omega A_{||} \nabla_{||} q^\varepsilon \cdot \nabla_{||} w \, dx = 0, & \forall w \in \mathcal{L} \,. \end{cases} \tag{13}$$

System (13) is an equivalent reformulation (for fixed $\varepsilon > 0$) of the original P-problem (9). Indeed, if $u^\varepsilon \in \mathcal{V}$ solves (9), then we can construct $q^\varepsilon \in \mathcal{L}$ such that $\nabla_{||} q^\varepsilon = (1/\varepsilon) \nabla_{||} u^\varepsilon$, cf. Lemma 4 below. Indeed, for this observe that

$$q \in \mathcal{L} \longmapsto \nabla_{||} q \in L^2(\Omega) \,,$$

is a one to one mapping. This, in weak form, gives the second equation of (13). Replacing then $\nabla_{||} u^\varepsilon$ by $\varepsilon \nabla_{||} q^\varepsilon$ inside (9), we see that $(u^\varepsilon, q^\varepsilon)$ solves also the first equation in (13). Conversely, if (13) has a solution $(u^\varepsilon, q^\varepsilon) \in \mathcal{V} \times \mathcal{L}$ then the second equation implies $\varepsilon \nabla_{||} q^\varepsilon = \nabla_{||} u^\varepsilon$, which inserted in the first one, leads to the weak formulation (9).

This proves that the MM-formulation (13) has a unique solution $(u^\varepsilon, q^\varepsilon) \in \mathcal{V} \times \mathcal{L}$ for all $\varepsilon > 0$ and $f \in L^2(\Omega)$, where $u^\varepsilon \in \mathcal{V}$ is the unique solution of the P-problem (9). The advantage of (13) over (9) consists in the fact that taking formally the limit $\varepsilon \to 0$ in (13) leads to the correct limit problem (11). Indeed, setting $\varepsilon = 0$ in the MM-formulation (13), we obtain the following problem (referred hereafter as the L-model): Find $(u^0, q^0) \in \mathcal{V} \times \mathcal{L}$ such that

$$(L) \quad \begin{cases} \displaystyle\int_\Omega (A_\perp \nabla_\perp u^0) \cdot \nabla_\perp v \, dx + \int_\Omega A_{||} \nabla_{||} q^0 \cdot \nabla_{||} v \, dx = \int_\Omega f v \, dx, & \forall v \in \mathcal{V} \\ \displaystyle\int_\Omega A_{||} \nabla_{||} u^0 \cdot \nabla_{||} w \, dx = 0, & \forall w \in \mathcal{L} \,. \end{cases} \tag{14}$$

Remark that (14) is formally an equivalent formulation of the Limit problem (11). In particular, if $(u^0, q^0) \in \mathcal{V} \times \mathcal{L}$ is a solution of (14), then $u^0 \in \mathcal{G}$, where $\mathcal{G}$ is defined in (8) and u^0 solves (11). The additional unknown q^0 serves here as the Lagrange multiplier responsible for the constraint $u^0 \in \mathcal{G}$. The existence of this Lagrange multiplier $q^0 \in \mathcal{L}$ is not completely straight-forward to prove, since we do not have an inf-sup property for the bilinear form $a_{||}$ on the pair of spaces $\mathcal{V} \times \mathcal{L}$. Fortunately, we can prove the existence assuming $f \in L^2(\Omega)$, cf. Theorem 3, thus establishing rigorously the equivalence between (11) and (14), at least for $f \in L^2(\Omega)$. This shall be part of the aim of the next subsection. The uniqueness is given by

Lemma 1 *Suppose that Hypothesis A is satisfied, in particular that $f \in L^2(\Omega)$. Then the solution to (14), if it exists, is unique.*

Proof. It is sufficient, due to linearity, to consider $f = 0$. Let thus $(u^0, q^0) \in \mathcal{V} \times \mathcal{L}$ be the solution of (14) for $f = 0$. Taking then test functions $v \in \mathcal{G}$, we get immediately $u^0 = 0$, implying $a_{||}(q^0, v) = 0$ for all $v \in \mathcal{V}$. By density arguments one gets then $q^0 = 0$. ■

Remark 2 *In the previous paper [6] we used the decomposition $u^\varepsilon = p^\varepsilon + q^\varepsilon$ for the construction of the duality-based AP-scheme, where $p \in \mathcal{G}$ and $q \in \mathcal{A}$, with $\mathcal{A}$ the space of functions with zero average along the field lines. In the present paper we have a slightly different decomposition $u^\varepsilon = p^\varepsilon + \varepsilon q^\varepsilon$ hidden in (9). The space $\mathcal{A}$ was replaced by the space $\mathcal{L}$ of functions vanishing on the inflow boundary. In the previous version, q^ε was useless in the limit $\varepsilon \to 0$, now it is a meaningfull Lagrange multiplier in this limit. Indeed, we prove in Theorem 3 below that $q^\varepsilon \to q^0$ as $\varepsilon \to 0$. This is the main reason why our new Micro-Macro AP-reformulation is more economical than the old Duality-based AP-reformulation.*

2.3 The behaviour of the MM-problem as $\varepsilon \to 0$

The objective of this subsection is to study the behaviour of the MM-solution $(u^\varepsilon, q^\varepsilon) \in \mathcal{V} \times \mathcal{L}$ of system (13) in the limit $\varepsilon \to 0$, in particular to show that it tends (in some sense) towards $(u^0, q^0) \in \mathcal{V} \times \mathcal{L}$, solution of the Limit model (14). In order to prove rigorously these results, we will suppose the following hypothesis on the domain that tells us essentially that Ω is a tube composed of field lines of b.

Hypothesis B *There exists a smooth coordinate system $(\xi_1, \dots, \xi_n)$ on Ω with $(\xi_1, \dots, \xi_{n-1}) \in D$, $\xi_n \in (0,1)$, D being a smooth domain in $\mathbb{R}^{n-1}$, such that the field lines of b are given by the coordinate lines $(\xi_1, \dots, \xi_{n-1}) = const$. Moreover, Γ_{in} is represented by $\xi_n = 0$, $(\xi_1, \dots, \xi_{n-1}) \in D$; Γ_{out} is represented by $\xi_n = 1$, $(\xi_1, \dots, \xi_{n-1}) \in D$ and Γ_D is represented by $\xi_n \in (0,1)$, $(\xi_1, \dots, \xi_{n-1}) \in \partial D$.*

We proved in [6] that such a coordinate system exists provided the components of the boundaries Γ_{in} and Γ_{out} admit smooth parametrizations and that b penetrates Γ_{in} and Γ_{out} at an angle that stays away from 0.

In the following we suppose that Hypotheses A and B hold true. We are then able to prove the following

Theorem 3 *Let Hypothesis A and B be statisfied and moreover suppose that $A_\perp \in \mathbb{M}_{d\times d}(W^{2,\infty}(\Omega))$ and $A_{||} \in W^{2,\infty}(\Omega)$. Then the MM-problem (13) admits a unique solution $(u^\varepsilon, q^\varepsilon) \in \mathcal{V} \times \mathcal{L}$ for any $\varepsilon > 0$, where u^ε is the unique solution of problem (9). There exists also a unique solution $(u^0, q^0) \in \mathcal{V} \times \mathcal{L}$ of the L-problem (14), where $u^0 \in \mathcal{G}$ solves problem (11). Moreover, we have the following convergences as $\varepsilon \to 0$*

$$u^\varepsilon \to u^0 \quad in \quad \mathcal{V}, \qquad q^\varepsilon \rightharpoonup q^0 \quad in \quad \mathcal{L},$$

and the following bounds hold

$$||\nabla_\perp u^\varepsilon - \nabla_\perp u^0||_{L^2} \leq C\sqrt{\varepsilon}||f||_{L^2}\,, \quad ||\nabla_{||} u^\varepsilon||_{L^2} \leq C\varepsilon\,||f||_{L^2} \;\; \textit{and} \;\; ||\nabla_{||} q^\varepsilon||_{L^2} \leq C||f||_{L^2}\,.$$

with a constant $C > 0$ independent of ε and f.

The proof of this theorem will use several lemmas which we prove first.

Lemma 4 *For any $u \in H^1(\Omega)$ and $\varepsilon > 0$, there exists a unique $q \in \mathcal{L}$ satisfying $\varepsilon\nabla_{||} q = \nabla_{||} u$ a.e. Moreover, if $u \in H^2(\Omega)$ then $q \in H^1(\Omega)$ and if $u \in \mathcal{V} \cap H^2(\Omega)$ then $q \in \mathcal{V}$.*

Proof. The idea of the proof is simply to say that q is constructed by subtracting from u its value on the inflow Γ_{in} on each field line and dividing the result by ε. More formally speaking, let us introduce the operator J that takes any function ϕ on Γ_{in} and returns the function $p = J\phi$, which coincides with ϕ on Γ_{in} and is constant on the field lines. In the coordinate system introduced in Hypothesis B, the definition of the operator J resumes to the following formula

$$(J\phi)(\xi_1, \ldots, \xi_{n-1}, \xi_n) = \phi(\xi_1, \ldots, \xi_{n-1}).$$

This implies (going from the coordinates ξ to the original ones) that J maps $L^2(\Gamma_{in})$ to $L^2(\Omega)$, $H^1(\Gamma_{in})$ to $H^1(\Omega)$ and $H^1_0(\Gamma_{in})$ to $\mathcal{V}$. Let us now define, for given u, the function $q = (u - J(u|_{\Gamma_{in}}))/\varepsilon$. Consequently, if $u \in H^1(\Omega)$ then $u|_{\Gamma_{in}} \in L^2(\Gamma_{in})$ and $q \in L^2(\Omega)$. If $u \in H^2(\Omega)$ then $u|_{\Gamma_{in}} \in H^1(\Gamma_{in})$ and $q \in H^1(\Omega)$. If, moreover, u vanishes on Γ_D then $u|_{\Gamma_{in}} \in H^1_0(\Gamma_{in})$ and $q \in \mathcal{V}$. ■

Lemma 5 *Let Hypothesis A and B be statisfied and moreover suppose that $A_\perp \in \mathbb{M}_{d\times d}(W^{2,\infty}(\Omega))$ and $A_{||} \in W^{2,\infty}(\Omega)$. Then the solution $u^0 \in \mathcal{G}$ of (11) belongs to $H^2(\Omega)$ and satisfies the estimates*

$$||u^0||_{H^2} \leq C||f||_{L^2}\,, \tag{15}$$

with a constant C independent of f.

Proof. Since u^0 is constant along the field lines, it is represented by $u^0(\xi_1, \ldots, \xi_{n-1})$ in the notations of Hypothesis B. The same is true for the test functions v in (11). Rewriting (11) in the ξ-coordinates gives

$$\sum_{1\leq i,j\leq n} \sum_{1\leq k,l\leq n-1} \int_{D\times(0,1)} A_{\perp,ij} \frac{\partial \xi_k}{\partial x_i} \frac{\partial \xi_l}{\partial x_j} \frac{\partial u^0}{\partial \xi_k} \frac{\partial v}{\partial \xi_l} \left|\frac{\partial x}{\partial \xi}\right| d\xi = \int_{D\times(0,1)} fv \left|\frac{\partial x}{\partial \xi}\right| d\xi$$

Introducing the positive definite matrix $C_{kl} = \sum_{1\leq i,j\leq n} A_{\perp,ij} \frac{\partial \xi_k}{\partial x_i} \frac{\partial \xi_l}{\partial x_j} \left|\frac{\partial x}{\partial \xi}\right|$ and integrating on ξ_n over $(0,1)$ yields

$$\sum_{1\leq k,l\leq n-1} \int_D C_{kl} \frac{\partial u^0}{\partial \xi_k} \frac{\partial v}{\partial \xi_l} d\xi_1 \cdots d\xi_{n-1} = \int_{D\times(0,1)} fv \left|\frac{\partial x}{\partial \xi}\right| d\xi.$$

We see that it is the weak formulation of an elliptic equation for u^0 on D with the boundary conditions $u^0 = 0$ on ∂D. By regularity results for elliptic equations, we see immediately that $u^0 \in H^2(D)$ if $f \in L^2(\Omega)$ with continuous dependence of u^0 on f. Reminding that u^0 does not depend on ξ_n and going back to the original coordinates yields (15). ■

Proof of Theorem 3. The existence and uniqueness of a solution of the MM-problem (13) was shown in the previous section. Note that u^ε is in fact in $H^2(\Omega)$ by the regularity results for elliptic equations since u^ε solves (4). Moreover, $q^\varepsilon \in \mathcal{V}$ thanks to Lemma 4.

Taking in the first equation of (13) test functions $v \in \mathcal{G}$, we deduce

$$a_\perp(u^\varepsilon, v) = (f, v) = a_\perp(u^0, v), \quad \forall v \in \mathcal{G}\,.$$

Choose now $v := u^\varepsilon - \varepsilon q^\varepsilon - u^0$ where $u^0 \in \mathcal{G}$ is the unique solution of (11). Thanks to the second eqaution in (13), $\nabla_{||} v = 0$ a.e. in Ω so that $v \in \mathcal{G}$. Substituting it in the equation above gives

$$a_\perp(u^\varepsilon, u^\varepsilon - \varepsilon q^\varepsilon - u^0) = a_\perp(u^0, u^\varepsilon - \varepsilon q^\varepsilon - u^0)\,,$$

implying

$$a_\perp(u^\varepsilon - u^0, u^\varepsilon - u^0) - \varepsilon a_\perp(u^\varepsilon, q^\varepsilon) = -\varepsilon a_\perp(u^0, q^\varepsilon). \tag{16}$$

Take now $v := \varepsilon q^\varepsilon$ in the first equation of (13) and add it to (16). This yields

$$a_\perp(u^\varepsilon - u^0, u^\varepsilon - u^0) + \varepsilon a_{||}(q^\varepsilon, q^\varepsilon) = \varepsilon(f, q^\varepsilon) - \varepsilon a_\perp(u^0, q^\varepsilon). \tag{17}$$

Since $u^0 \in H^2(\Omega)$ by Lemma 5 we can integrate by parts in $a_\perp(u^0, q^\varepsilon)$:

$$\begin{aligned}
-a_\perp(u^0, q^\varepsilon) &= -\int_\Omega \left(A_\perp \nabla_\perp u^0\right) \cdot \nabla_\perp q^\varepsilon dx = -\int_\Omega \left[(Id - b\otimes b) A_\perp \nabla u^0\right] \cdot \nabla q^\varepsilon dx \\
&= -\int_{\Gamma_{out}} \left[(Id - b\otimes b) A_\perp \nabla u^0\right] \cdot n q^\varepsilon d\sigma + \int_\Omega \left[\nabla \cdot ((Id - b\otimes b) A_\perp \nabla u^0)\right] q^\varepsilon dx \\
&\le C||u^0||_{H^2(\Omega)} \left(||q^\varepsilon||_{L^2(\Gamma_{out})} + ||q^\varepsilon||_{L^2(\Omega)}\right)
\end{aligned}$$

since ∇u^0 has a trace on Γ_{out} and its norm in $L^2(\Gamma_{out})$ is bounded by $C||u^0||_{H^2(\Omega)}$. Thus, (17) tells us

$$||\nabla_{||} q^\varepsilon||^2_{L^2(\Omega)} \le C a_{||}(q^\varepsilon, q^\varepsilon) \le C||f||_{L^2}||q^\varepsilon||_{L^2(\Omega)} + C||u^0||_{H^2(\Omega)} \left(||q^\varepsilon||_{L^2(\Gamma_N)} + ||q^\varepsilon||_{L^2(\Omega)}\right).$$

By the Poincaré and trace inequalities (proved easily by passing to the ξ-coordinates of Hypothesis B) and by Lemma 5, we have

$$||q^\varepsilon||_{L^2(\Omega)} \le C||\nabla_{||} q^\varepsilon||_{L^2(\Omega)}, \quad ||q^\varepsilon||_{L^2(\Gamma_{out})} \le C||\nabla_{||} q^\varepsilon||_{L^2(\Omega)}, \text{ and } ||u^0||_{H^2(\Omega)} \le C||f||_{L^2(\Omega)}$$

so that

$$||\nabla_{||} q^\varepsilon||_{L^2(\Omega)} \le C||f||_{L^2(\Omega)}.$$

This gives immediately also the estimate $||\nabla_{||} u^\varepsilon||_{L^2} \le C\varepsilon||f||_{L^2}$ since $\nabla_{||} u^\varepsilon = \varepsilon \nabla_{||} q^\varepsilon$. Returning to (17), we observe that

$$||\nabla_\perp u^\varepsilon - \nabla_\perp u^0||^2_{L^2} \le \varepsilon(f, q^\varepsilon) - \varepsilon a_\perp(u^0, q^\varepsilon) \le C\varepsilon||f||^2_{L^2(\Omega)}\,,$$

so that all the estimates are proved. They imply immediately the strong convergence $u^\varepsilon \to u^0$ in $H^1(\Omega)$.

It remains to prove the weak convergence of q^ε and existence of q^0 that solves (14). Since the familly of functions q^ε is bounded in $\mathcal{L}$, there is a subsequence q^{ε_n} weakly converging to some $q^0 \in \mathcal{L}$ as $\varepsilon_n \to 0$. Taking the limit $\varepsilon_n \to 0$ in (13), we see that (u^0, q^0) solves (14). We know already that the solution (u^0, q^0) is unique, cf. Lemma 1. It means that any converging sequence q^{ε_n} (with $\varepsilon_n \to 0$) has q^0 as its limit. Hence, $q^\varepsilon \rightharpoonup q^0$ as $\varepsilon \to 0$. This finishes the proof. ■

The next theorem shows some nice H^2-regularity results for the unique solution $u^\varepsilon \in \mathcal{V}$ of the P-problem (9). This result is proven for the moment only for a simplified geometry: $\Omega := (0, L_x) \times (0, L_y)$ and $b = (0, 1)$ assumed constant and aligned in the y direction. Let us thus study the system

$$\begin{cases}
-\frac{1}{\varepsilon}\partial_y(A_y \partial_y u^\varepsilon) - \partial_x(A_x \partial_x u^\varepsilon) = f\,, & \text{in } \Omega \\
\partial_y u^\varepsilon = 0\,, & \text{for } y = 0, L_y \\
u^\varepsilon = 0\,, & \text{for } x = 0, L_x\,.
\end{cases} \tag{18}$$

Theorem 6 *Take $\Omega := (0, L_x) \times (0, L_y)$, $b = (0, 1)$, suppose that Hypothesis A is satisfied and moreover that $A_x = (A_\perp)_{11} \in W^{2,\infty}(\Omega)$ and $A_y = A_{||} \in W^{2,\infty}(\Omega)$. Then u^ε, the unique solution of (18), belongs to $H^2(\Omega)$ and we have the estimates*

$$||\partial_x u^\varepsilon||^2_{L^2} + \frac{1}{\varepsilon^2}||\partial_y u^\varepsilon||^2_{L^2} \leq C||f||^2_{L^2}\,, \tag{19}$$

$$||\partial_{xx} u^\varepsilon||^2_{L^2} + \frac{1}{\varepsilon}||\partial_{xy} u^\varepsilon||^2_{L^2} + \frac{1}{\varepsilon^2}||\partial_{yy} u^\varepsilon||^2_{L^2} \leq C||f||^2_{L^2}\,, \tag{20}$$

with $C > 0$ a constant independent of ε and f.

Remark 7 *The estimate (19) is already proven in Theorem 3 in a more general context. However, we provide below an alternative proof for it, which consists in the interplay with the estimates for the second derivatives and which does not require the Lemmas proven above. This alternative proof is thus simpler than that of Theorem 3 presented above, but it is not straight forward to generalize it to the case of an arbitrary geometry of Ω and an arbitrary field b.*

Proof of Theorem 6. Standard elliptic results permit to show, under the additional hypothesis of this theorem, that $u^\varepsilon \in H^2(\Omega)$.

First remark that multiplying the equation by u^ε, integrating over Ω yields immediately by integration by parts the H^1-estimate

$$\frac{1}{\varepsilon}||\nabla_y u^\varepsilon||^2_{L^2} + ||\nabla_x u^\varepsilon||^2_{L^2} \leq C||f||^2_{L^2}\,. \tag{21}$$

Rewriting now the equation as

$$-\frac{1}{\varepsilon}A_y\partial_{yy}u^\varepsilon - A_x\partial_{xx}u^\varepsilon = f + \frac{1}{\varepsilon}(\partial_y A_y)\partial_y u^\varepsilon + (\partial_x A_x)\partial_x u^\varepsilon\,,$$

multiplying it by $-\partial_{yy}u^\varepsilon - \partial_{xx}u^\varepsilon$ and integrating over Ω yields (by integration by parts)

$$\begin{aligned}
&\tfrac{1}{\varepsilon}||\sqrt{A_y}\partial_{yy}u^\varepsilon||^2 + \tfrac{1}{\varepsilon}||\sqrt{A_y}\partial_{xy}u^\varepsilon||^2 + ||\sqrt{A_x}\partial_{xy}u^\varepsilon||^2 + ||\sqrt{A_x}\partial_{xx}u^\varepsilon||^2 \\
&\qquad \leq C\left[||f||\left(||\partial_{xx}u^\varepsilon|| + ||\partial_{yy}u^\varepsilon||\right) + \tfrac{1}{\varepsilon}\left(||\partial_y u^\varepsilon||\,||\partial_{xy}u^\varepsilon|| + ||\partial_y u^\varepsilon||\,||\partial_{yy}u^\varepsilon||\right) + ||\partial_x u^\varepsilon||\left(||\partial_{xy}u^\varepsilon|| + ||\partial_{xx}u^\varepsilon||\right)\right]
\end{aligned}$$

Using now the H^1-estimate (21), in particular that $||\partial_y u^\varepsilon|| \leq C\sqrt{\varepsilon}||f||$ one gets

$$\begin{aligned}
&\tfrac{1}{\varepsilon}||\sqrt{A_y}\partial_{yy}u^\varepsilon||^2 + \tfrac{1}{\varepsilon}||\sqrt{A_y}\partial_{xy}u^\varepsilon||^2 + ||\sqrt{A_x}\partial_{xy}u^\varepsilon||^2 + ||\sqrt{A_x}\partial_{xx}u^\varepsilon||^2 \\
&\qquad \leq C||f||\left(||\partial_{xx}u^\varepsilon|| + ||\partial_{yy}u^\varepsilon|| + \tfrac{1}{\sqrt{\varepsilon}}||\partial_{xy}u^\varepsilon|| + \tfrac{1}{\sqrt{\varepsilon}}||\partial_{yy}u^\varepsilon|| + ||\partial_{xy}u^\varepsilon||\right)\,,
\end{aligned}$$

yielding immediately by Young inequality

$$\tfrac{1}{\varepsilon}||\partial_{yy}u^\varepsilon||^2 + \tfrac{1}{\varepsilon}||\partial_{xy}u^\varepsilon||^2 + ||\partial_{xx}u^\varepsilon||^2 \leq C||f||^2\,.$$

Coming now back to the equation

$$-\frac{1}{\varepsilon}\partial_y(A_y\partial_y u^\varepsilon) = f + \partial_x(A_x\partial_x u^\varepsilon)\,,$$

one gets with the last estimates

$$\frac{1}{\varepsilon}||\partial_y(A_y\partial_y u^\varepsilon)|| \leq C||f||\,.$$

Poincaré's inequality permits then to estimate

$$||A_y\partial_y u^\varepsilon|| \leq C||\partial_y(A_y\partial_y u^\varepsilon)|| \leq C\varepsilon||f||\,,$$

yielding $||\partial_y u^\varepsilon|| \leq C\varepsilon||f||$ and thus (19). Coming again back to the equation

$$-\frac{1}{\varepsilon}A_y\partial_{yy}u^\varepsilon = f + \partial_x(A_x\partial_x u^\varepsilon) + \frac{1}{\varepsilon}(\partial_y A_y)\partial_y u^\varepsilon\,,$$

permits to show (20) and to conclude the proof. ■

3 Numerical results

This section is devoted to the numerical simulation of the anisotropic P-problem (4) via the here introduced MM-scheme and to the numerical illustration of its advantages.

3.1 A finite element discretization

Let us introduce a discretization of the domain Ω of size h and a finite element space $\mathcal{V}_h$ of type $\mathbb{P}_k$ or $\mathbb{Q}_k$ on this mesh. We assume that the boundary conditions on Γ_D are enforced in the definition of $\mathcal{V}_h$, i.e. $\mathcal{V}_h \subset \mathcal{V}$. Consider then the subspace $\mathcal{L}_h$ of $\mathcal{V}_h$ defined by $\mathcal{L}_h = \mathcal{V}_h \cap \mathcal{L}$

$$\mathcal{L}_h = \{q_h \in \mathcal{V}_h\,,\ \text{such that } q_h|_{\Gamma_{in}} = 0\}.$$

This choice is explained in more details in our previous paper [6]. The standard discretization of (13) writes then: find $(u_h^\varepsilon, q_h^\varepsilon) \in \mathcal{V}_h \times \mathcal{L}_h$ such that

$$(MM)_h \quad \begin{cases} a_\perp(u_h^\varepsilon, v_h) + a_{||}(q_h^\varepsilon, v_h) = \int_\Omega f v_h\, dx, \quad \forall v_h \in \mathcal{V}_h \\ a_{||}(u_h^\varepsilon, w_h) - \varepsilon a_{||}(q_h^\varepsilon, w_h) = 0, \quad \forall w_h \in \mathcal{L}_h\,. \end{cases} \tag{22}$$

This section concerns the detailed study of the obtained numerical results. In particular, we compare the method presented herein with the duality-based AP-approach developed in our previous article [6] and present the convergence of the new scheme for an arbitrary anisotropy field b and constant ε test case, the convergence being uniform in ε. The detailed numerical analysis shall be presented in a forthcoming work.

3.2 Discretization

Let us present, for simplicity, the discretization in a 2D case, the 3D case being a simple extension. The here considered computational domain Ω is a square $\Omega = [0,1] \times [0,1]$. All simulations are performed on structured meshes. Let us introduce the Cartesian, homogeneous grid

$$x_i = i/N_x \ \ , \ \ 0 \le i \le N_x\,, \quad y_j = j/N_y \ \ , \ \ 0 \le j \le N_y, \tag{23}$$

where N_x and N_y are positive even constants, corresponding to the number of discretization intervals in the x- resp. y-direction. The corresponding mesh-sizes are denoted by $h_x > 0$ resp. $h_y > 0$. Choosing a $\mathbb{Q}_2$ finite element method ($\mathbb{Q}_2$-FEM), based on the following quadratic base functions

$$\theta_{x_i} = \begin{cases} \frac{(x-x_{i-2})(x-x_{i-1})}{2h_x^2} & x \in [x_{i-2}, x_i], \\ \frac{(x_{i+2}-x)(x_{i+1}-x)}{2h_x^2} & x \in [x_i, x_{i+2}], \\ 0 & \text{else} \end{cases} \ , \quad \theta_{y_j} = \begin{cases} \frac{(y-y_{j-2})(y-y_{j-1})}{2h_y^2} & y \in [y_{j-2}, y_j], \\ \frac{(y_{j+2}-y)(y_{j+1}-y)}{2h_y^2} & y \in [y_j, y_{j+2}], \\ 0 & \text{else} \end{cases} \tag{24}$$

for even i, j and

$$\theta_{x_i} = \begin{cases} \frac{(x_{i+1}-x)(x-x_{i-1})}{h_x^2} & x \in [x_{i-1}, x_{i+1}], \\ 0 & \text{else} \end{cases} \ , \quad \theta_{y_j} = \begin{cases} \frac{(y_{j+1}-y)(y-y_{j-1})}{h_y^2} & y \in [y_{j-1}, y_{j+1}], \\ 0 & \text{else} \end{cases} \tag{25}$$

for odd i, j, we define

$$W_h := \{v_h = \sum_{i,j} v_{ij}\, \theta_{x_i}(x)\, \theta_{y_j}(y)\}\,.$$

The spaces $\mathcal{V}_h$ and $\mathcal{L}_h$ are then defined by

$$\mathcal{V}_h = \{u_h \in \mathcal{W}_h \,,\ \text{such that } u_h|_{\Gamma_D} = 0\}\,, \quad \mathcal{L}_h = \{q_h \in \mathcal{V}_h \,,\ \text{such that } q_h|_{\Gamma_{in}} = 0\}.$$

The matrix elements are computed using the 2D Gauss quadrature formula, with 3 points in the x and y direction:

$$\int_{-1}^{1}\int_{-1}^{1} f(x,y) = \sum_{i,j=-1}^{1} \omega_i\omega_j f(x_i,y_j)\,, \tag{26}$$

where $x_0 = y_0 = 0$, $x_{\pm1} = y_{\pm1} = \pm\sqrt{\frac{3}{5}}$, $\omega_0 = 8/9$ and $\omega_{\pm1} = 5/9$, which is exact for polynomials of degree 5.

3.3 Duality-Based (DB) asymptotic-preserving method

In order to compare the new, here introduced, MM-reformulation (13) with the previously considered [6] duality-based AP-scheme, let us briefly recall the former one. This alternative approach is based on the following orthogonal decomposition of the solution of the original problem (4): $u = p + q$, where $p \in \mathcal{G}$ and $q \in \mathcal{A}$. The vector space

$$\mathcal{G} = \{u \in \mathcal{V} \mid \nabla_{\|} u = 0\}\,, \tag{27}$$

is the Hilbert space of functions, which are constant along the field lines of b and was introduced in (8). The vector space $\mathcal{A}$ is the L^2-orthogonal complement to $\mathcal{G}$ in $\mathcal{V}$, defined by

$$\mathcal{A} := \{u \in \mathcal{V} \mid \ (u,v) = 0 \ \ ,\ \ \forall v \in \mathcal{G}\}\,, \quad \mathcal{V} = \mathcal{G} \oplus^{\perp} \mathcal{A}\,. \tag{28}$$

Hence, the subspace $\mathcal{A}$ contains the functions that have zero average along the field lines b.

This decomposition leads to the system: find $(p^\varepsilon, q^\varepsilon) \in \mathcal{G} \times \mathcal{A}$ such that:

$$\begin{cases} a_\perp(p^\varepsilon,\eta) + a_\perp(q^\varepsilon,\eta) = (f,\eta) & \forall \eta \in \mathcal{G} \\ a_{||}(q^\varepsilon,\xi) + \varepsilon a_\perp(q^\varepsilon,\xi) + \varepsilon a_\perp(p^\varepsilon,\xi) = \varepsilon(f,\xi) & \forall \xi \in \mathcal{A} \end{cases}, \tag{29}$$

which is asymptotic-preserving, well-posed and well-conditioned regardless of the value of ε. The discretization of the vector spaces $\mathcal{A}$ and $\mathcal{G}$ is achieved by means of a Lagrange multiplier technique: first we explore the orthogonality of $\mathcal{A}$ and $\mathcal{G}$ in order to avoid the direct discretization of the space $\mathcal{A}$. The thus obtained system reads: find $(p^\varepsilon, q^\varepsilon, l^\varepsilon) \in \mathcal{G} \times \mathcal{V} \times \mathcal{G}$ such that

$$\begin{cases} a_\perp(p^\varepsilon,\eta) + a_\perp(q^\varepsilon,\eta) = (f,\eta) & \forall \eta \in \mathcal{G}, \\ a_{||}(q^\varepsilon,\xi) + \varepsilon a_\perp(q^\varepsilon,\xi) + \varepsilon a_\perp(p^\varepsilon,\xi) + (l^\varepsilon,\xi) = \varepsilon(f,\xi) & \forall \xi \in \mathcal{V}, \\ (q^\varepsilon,\chi) = 0 & \forall \chi \in \mathcal{G}, \end{cases} \tag{30}$$

where l^ε is a Lagrange multiplier. The additional term (l^ε,ξ) in the second equations allows us to replace the vector space $\mathcal{A}$ by $\mathcal{V}$. The third equation forces q^ε to belong to $\mathcal{A}$.

Afterwards, the definition of the space $\mathcal{G}$ is used to obtain a system which does not require the direct discretization of $\mathcal{G}$. The resulting system reads now: find $(p^\varepsilon,\ \lambda^\varepsilon,\ q^\varepsilon,\ l^\varepsilon,\ \mu^\varepsilon) \in \mathcal{V} \times \mathcal{L} \times \mathcal{V} \times$

$\mathcal{V} \times \mathcal{L}$ such that

$$(DB) \quad \begin{cases} a_\perp(p^\varepsilon, \eta) + a_\perp(q^\varepsilon, \eta) + a_{||}(\eta, \lambda^\varepsilon) = (f, \eta) \,, \quad \forall \eta \in \mathcal{V} \,, \\ a_{||}(p^\varepsilon, \kappa) = 0 \,, \quad \forall \kappa \in \mathcal{L} \,, \\ a_{||}(q^\varepsilon, \xi) + \varepsilon a_\perp(q^\varepsilon, \xi) + \varepsilon a_\perp(p^\varepsilon, \xi) + (l^\varepsilon, \xi) = \varepsilon\,(f, \xi) \,, \quad \forall \xi \in \mathcal{V} \,, \\ (q^\varepsilon, \chi) + a_{||}(\chi, \mu^\varepsilon) = 0 \,, \quad \forall \chi \in \mathcal{V} \,, \\ a_{||}(l^\varepsilon, \tau) = 0 \,, \quad \forall \tau \in \mathcal{L} \,, \end{cases} \tag{31}$$

with $\mathcal{L}$ being a Lagrange multiplier space defined by (12). Two additional Lagrange multipliers λ^ε and μ^ε are introduced in order to replace $\mathcal{G}$ by the bigger and easier to implement vector-space $\mathcal{V}$. For a more detailed presentation of the duality-based asymptotic preserving reformulation, we refer to [6].

This decomposition of the solution $u \in \mathcal{V}$ into two parts: a mean part $p \in \mathcal{G}$ and the fluctuating part $q \in \mathcal{A}$ with zero average along the field lines, may seem more intuitive than the new decomposition presented in this paper. This feature however has its drawbacks. The fact that we had to introduce three additional unknowns increases significantly the computational complexity of the problem. In the following, we compare the DB Asymptotic-Preserving approach (31) with the new MM Asymptotic-Preserving approach (13) and show that the new method is superior in terms of memory requirements and computational time, while the accuracy remains the same. In particular, we demonstrate that convergence is uniform in ε.

3.4 Numerical tests

3.4.1 2D test case, constant ε, uniform and aligned b-field

In this section we compare the numerical results obtained via the $\mathbb{Q}_2$-FEM described in Section 3.2, and applied to the Singular Perturbation model (4), the Duality-Based model (31) and the Micro-Macro reformulation (13). In all numerical tests we set $A_\perp = Id$ and $A_\parallel = 1$. We start with a simple test case, where the analytical solution is known. Let the source term f be given by

$$f = (4 + \varepsilon)\,\pi^2 \cos(2\pi x) \sin(\pi y) + \pi^2 \sin(\pi y) \tag{32}$$

and let the b field be aligned with the x-axis. Hence, the solution u^ε of (4) is given by

$$u^\varepsilon = \sin(\pi y) + \varepsilon \cos(2\pi x) \sin(\pi y)$$

We denote by u_P, u_D resp. u_A the numerical solutions of the Singular Perturbation model (4), the Duality-Based Asymptotic Preserving model (31) resp. the Micro-Macro Asymptotic Preserving reformulation (13). The comparison will be done in the L^2-norm as well as the H^1-norm. The linear systems obtained after discretization of the three methods are solved using the same numerical algorithm — LU decomposition implemented in a solver MUMPS[2].

In Figure 1 we plotted the absolute errors (in the L^2 resp. H^1-norms) between the numerical solutions obtained with one of the three methods and the exact solution, and this, as a function of the parameter ε and for several mesh-sizes. In Table 1, we specified the error values for one fixed grid and several ε-values. One observes that the Singular Perturbation finite element approximation is accurate only for ε bigger than some critical value ε_P while the MM-scheme and the DB-scheme are both accurate independently on ε and give similar results.
The order of convergence for all three methods is three in the L^2-norm and two in the H^1-norm, which is an optimal result for $\mathbb{Q}_2$ finite elements. The convergence of the MM-scheme is presented

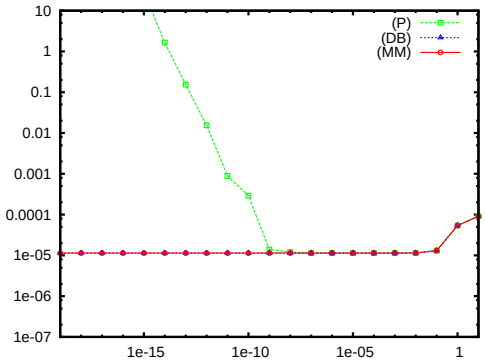

(a) L^2 error for a grid with 50×50 points.

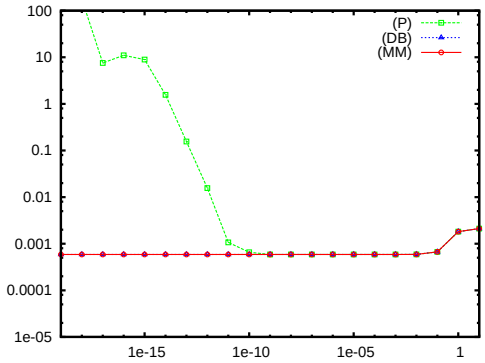

(b) H^1 error for a grid with 50×50 points.

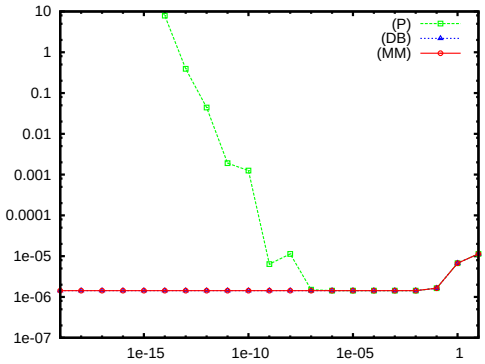

(c) L^2 error for a grid with 100×100 points.

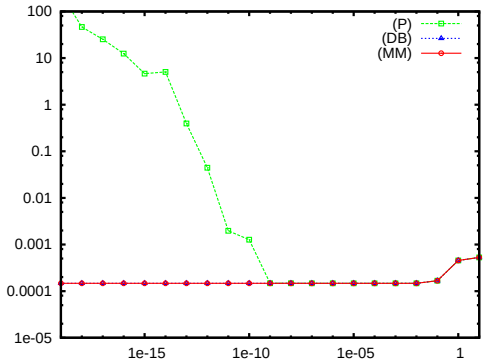

(d) H^1 error for a grid with 100×100 points.

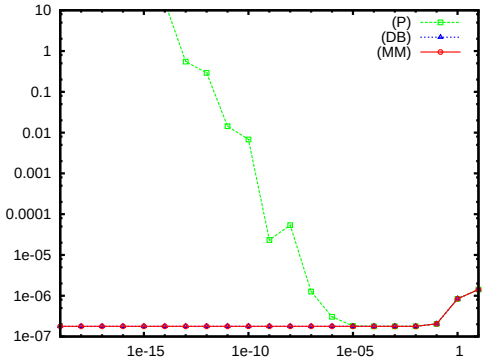

(e) L^2 error for a grid with 200×200 points.

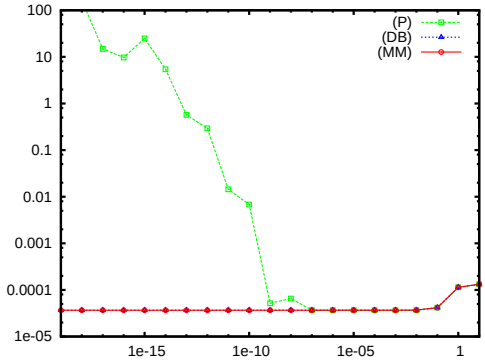

(f) H^1 error for a grid with 200×200 points.

Figure 1: Relative L^2 (left column) and H^1 (right column) errors between the exact solution u^ε and the computed numerical solutions u_M (MM), u_D (DB), u_P (P) for the test case with constant b. The error is plotted as a function of the parameter ε and for three different mesh-sizes.

ε	MM scheme		DB scheme		Singular Perturbation scheme	
	L^2 error	H^1 error	L^2 error	H^1 error	L^2 error	H^1 error
10	7.2×10^{-6}	4.7×10^{-3}	7.2×10^{-6}	4.7×10^{-3}	7.2×10^{-6}	4.7×10^{-3}
1	7.3×10^{-7}	4.7×10^{-4}	7.3×10^{-7}	4.7×10^{-4}	7.3×10^{-7}	4.7×10^{-4}
10^{-1}	1.47×10^{-7}	9.6×10^{-5}	1.47×10^{-7}	9.6×10^{-5}	1.45×10^{-7}	9.4×10^{-5}
10^{-4}	1.28×10^{-7}	8.3×10^{-5}	1.28×10^{-7}	8.3×10^{-5}	1.26×10^{-7}	8.2×10^{-5}
10^{-6}	1.28×10^{-7}	8.3×10^{-5}	1.28×10^{-7}	8.3×10^{-5}	5.9×10^{-7}	8.2×10^{-5}
10^{-10}	1.28×10^{-7}	8.3×10^{-5}	1.28×10^{-7}	8.3×10^{-5}	9.9×10^{-3}	3.12×10^{-2}
10^{-15}	1.28×10^{-7}	8.3×10^{-5}	1.28×10^{-7}	8.3×10^{-5}	7.1×10^{-1}	2.23×10^{0}

Table 1: Comparison between the Micro-Macro scheme, the Duality-Based reformulation and the Singular Perturbation model for $h = 0.005$ (200 mesh points in each direction) and constant b: absolute L^2-errors and H^1-errors, for different ε-values.

method	# rows	# non zero	time	L^2-error	H^1-error
MM	20×10^3	623×10^3	1.156 s	1.19×10^{-6}	1.47×10^{-4}
DB	50×10^3	1563×10^3	7.405 s	1.19×10^{-6}	1.47×10^{-4}
P	10×10^3	255×10^3	0.501 s	1.19×10^{-6}	1.47×10^{-4}

Table 2: Comparison between the Micro-Macro AP-scheme (MM), the Duality-Based AP-scheme (DB) and the Singular Perturbation model (P) for $h = 0.01$ (100 mesh points in each direction) and fixed $\varepsilon = 10^{-6}$: matrix size, number of nonzero elements, average computational time and relative error in L^2 and H^1 norms.

on Tables 3 and 4.
Furthermore the condition number of the MM-scheme is bounded by an ε independent constant and coincides with the condition number of DB-scheme for $\varepsilon < 0.1$. See Figure 2 for the plots.

Since both Asymptotic Preserving models (DB/MM) give the same accuracy in this test case, it is worthwhile to compare the computational resources required to obtain this same results. The computational time and the matrix sizes required to solve the problem for fixed ε and h are given in the Table 2. As expected, the MM-scheme is more efficient than the DB-approach. The average computational time of the MM-scheme is approximately 6.4 times smaller as compared to the DB-simulation time. It should be noted that the Singular Perturbation model is approximately 2.3 faster than the new MM-method. However, the applicability of the Singular Perturbation scheme is limited to sufficiently large values of ε.

3.4.2 2D test case, constant ε, non-uniform and non-aligned b-field

We now focus our attention on the original feature of the here introduced numerical method, namely its ability to treat nonuniform b fields. In this section we present numerical simulations performed for a variable field b.

First, let us construct a numerical test case. Finding an analytical solution for an arbitrary b-field presents a considerable difficulty. In the previous paper [6], we presented a way to find such

h	L^2-error in u	H^1-error in u	L^2-error in q	H^1-error in q
0.1	5.7×10^{-3}	1.86×10^{-1}	5.7×10^{-3}	1.86×10^{-1}
0.05	7.3×10^{-4}	4.7×10^{-2}	7.3×10^{-4}	4.7×10^{-2}
0.025	9.1×10^{-5}	1.18×10^{-2}	9.1×10^{-5}	1.18×10^{-2}
0.0125	1.14×10^{-5}	2.96×10^{-3}	1.14×10^{-5}	2.96×10^{-3}
0.00625	1.43×10^{-6}	7.4×10^{-4}	1.43×10^{-6}	7.4×10^{-4}
0.003125	1.78×10^{-7}	1.85×10^{-4}	1.78×10^{-7}	1.85×10^{-4}
0.0015625	2.23×10^{-8}	4.6×10^{-5}	2.23×10^{-8}	4.6×10^{-5}

Table 3: The absolute error of u and q in L^2 and H^1-norms for different mesh sizes and $\varepsilon = 1$. Used discretization method: Micro-Macro scheme (MM).

h	L^2-error in u	H^1-error in u	L^2-error in q	H^1-error in q
0.1	1.00×10^{-3}	3.25×10^{-2}	5.7×10^{-3}	1.86×10^{-1}
0.05	1.26×10^{-4}	8.2×10^{-3}	7.3×10^{-4}	4.7×10^{-2}
0.025	1.58×10^{-5}	2.04×10^{-3}	9.1×10^{-5}	1.18×10^{-2}
0.0125	1.97×10^{-6}	5.1×10^{-4}	1.14×10^{-5}	2.96×10^{-3}
0.00625	2.46×10^{-7}	1.28×10^{-4}	1.43×10^{-6}	7.4×10^{-4}
0.003125	3.1×10^{-8}	3.2×10^{-5}	2.59×10^{-5}	2.96×10^{-2}
0.0015625	4.1×10^{-9}	8.0×10^{-6}	4.0×10^{-4}	9.1×10^{-1}

Table 4: The absolute error of u and q in L^2 and H^1-norms for different mesh sizes and $\varepsilon = 10^{-100}$. Used discretization method: Micro-Macro scheme (MM).

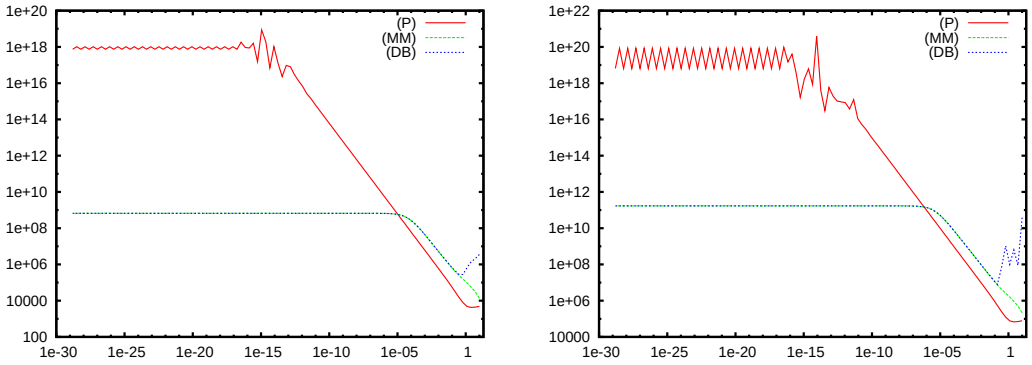

(a) mesh size: 100×100 points (b) mesh size: 400×400 points

Figure 2: Condition number estimate provided by the MUMPS solver for the (MM), (DB) and (P) schemes.

a solution. Let us recall briefly how to do. First, we choose a limit solution

$$u^0 = \sin\left(\pi y + \alpha(y^2 - y)\cos(\pi x)\right), \tag{33}$$

where α is a numerical constant aimed to control the variations of b. For $\alpha = 0$, the limit solution of the previous section is obtained. The limit solution for $\alpha = 2$ is shown in Figure 4. Since u^0 is a limit solution, it is constant along the b field lines. Therefore we can determine the b field using the following implication

$$\nabla_\parallel u^0 = 0 \quad \Rightarrow \quad b_x \frac{\partial u^0}{\partial x} + b_y \frac{\partial u^0}{\partial y} = 0, \tag{34}$$

which yields for example

$$b = \frac{B}{|B|}, \quad B = \begin{pmatrix} \alpha(2y-1)\cos(\pi x) + \pi \\ \pi\alpha(y^2 - y)\sin(\pi x) \end{pmatrix}. \tag{35}$$

Note that the field B, constructed in this way, satisfies $\mathrm{div} B = 0$, which is an important property in the framework of plasma simulations. Furthermore, we have $B \neq 0$ in the computational domain. Now, we choose u^ε to be a function that converges, as $\varepsilon \to 0$, to the limit solution u^0, for example

$$u^\varepsilon = \sin\left(\pi y + \alpha(y^2 - y)\cos(\pi x)\right) + \varepsilon \cos(2\pi x)\sin(\pi y)$$

Finally, the force term is calculated, using the equation, i.e.

$$f = -\nabla_\perp \cdot (A_\perp \nabla_\perp u^\varepsilon) - \frac{1}{\varepsilon}\nabla_\parallel \cdot (A_\parallel \nabla_\parallel u^\varepsilon).$$

The simulation results are presented on Figure 3. Similarly to the previous test case, both, the Micro-Macro Asymptotic Preserving approach and the Duality-Based Asymptotic Preserving reformulation, give the same accuracy. Both methods converge with the optimal rate in both L^2 and H_1 norms, independently of ε. The discretization of the Singular-Perturbation model is again limited. The critical value ε_P is now of the order of 10^{-2} and seems mesh independent while in the uniform b case this value ranged from 10^{-9} to 10^{-5} depending on the mesh size.

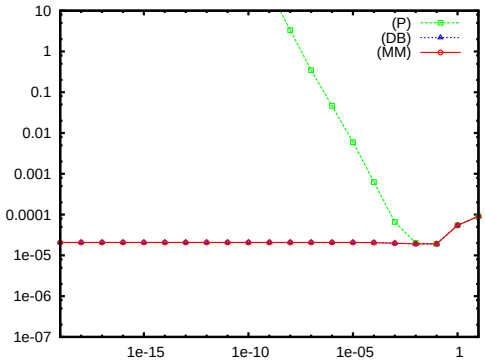

(a) L^2 error for a grid with 50×50 points.

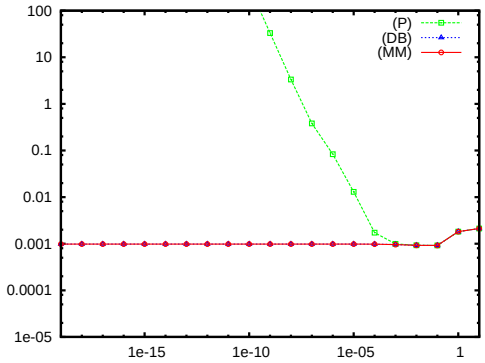

(b) H^1 error for a grid with 50×50 points.

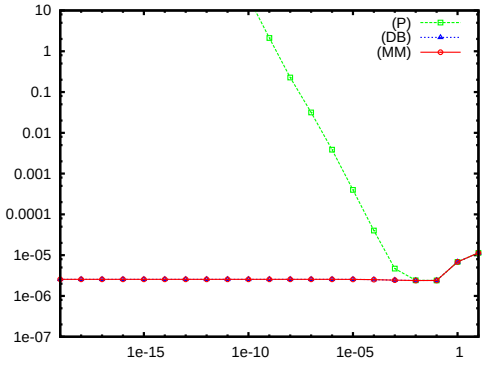

(c) L^2 error for a grid with 100×100 points.

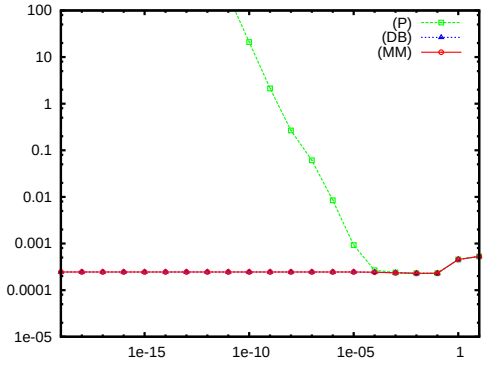

(d) H^1 error for a grid with 100×100 points.

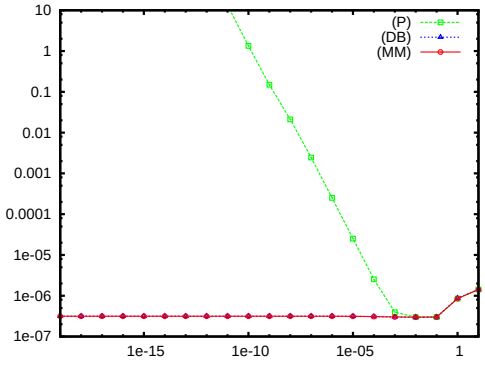

(e) L^2 error for a grid with 200×200 points.

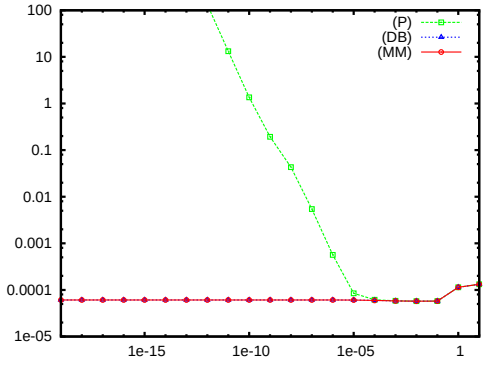

(f) H^1 error for a grid with 200×200 points.

Figure 3: Relative L^2 (left column) and H^1 (right column) errors between the exact solution u^ε and the computed solution u_M (MM), u_D (DB), u_P (P) for the test case with variable b. Plotted are the errors as a function of the small parameter ε, for three different meshes.

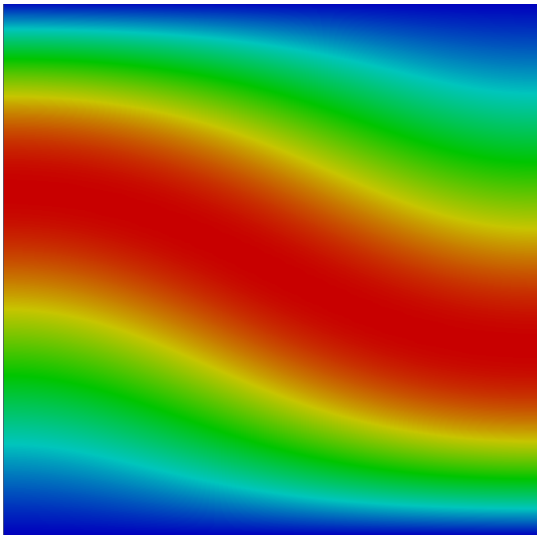

Figure 4: The limit solution for the test case with variable b.

It is worthwile to investigate the influence of the variations of the b-field on the accuracy of the solution. It is particularly interesting to find out the minimal number of mesh nodes per characteristic length of b-variations required to obtain an acceptable solution. For this, let us proceed as in the previous paper [6] and define a variant of the test case presented above.

Let $b = B/|B|$, with

$$B = \begin{pmatrix} \alpha(2y-1)\cos(m\pi x) + \pi \\ m\pi\alpha(y^2-y)\sin(m\pi x) \end{pmatrix}, \tag{36}$$

m being an integer. The limit solution ϕ^0 and ϕ^ε are chosen to be

$$\phi^0 = \sin\left(\pi y + \alpha(y^2-y)\cos(m\pi x)\right), \tag{37}$$

$$\phi^\varepsilon = \sin\left(\pi y + \alpha(y^2-y)\cos(m\pi x)\right) + \varepsilon\cos(2\pi x)\sin(\pi y). \tag{38}$$

As in [6], we perform numerical simulations on a fixed 400×400 grid ($h = 0.0025$) and vary m. We obtain the same results: the relative error in the L^2-norm, defined as $\frac{||u^\varepsilon - u_M||_{L^2(\Omega)}}{||u_M||_{L^2(\Omega)}}$, is below 0.01 for all tested values of $1 \leq m \leq 50$. The relative H^1-error $\frac{||u^\varepsilon - u_M||_{H^1(\Omega)}}{||u_M||_{H^1(\Omega)}}$ exceeds the critical value for $m > 25$. For $\varepsilon = 10^{-20}$ the maximal m for which the error is acceptable in both norms is 20. The minimal number of mesh points per period of b variations is 40 in the worst case, in order to obtain an 1% relative error. The results are summarized on Figures 5. The results prove that the MM-scheme is precise even for strongly oscillating fields for relatively small mesh sizes.

4 Generalization to the variable ε case

In this section we introduce a generalization of the Micro-Macro scheme to the case of an anisotropy intensity ε variable in space. The anisotropy parameter ε is now a function of space coordinates

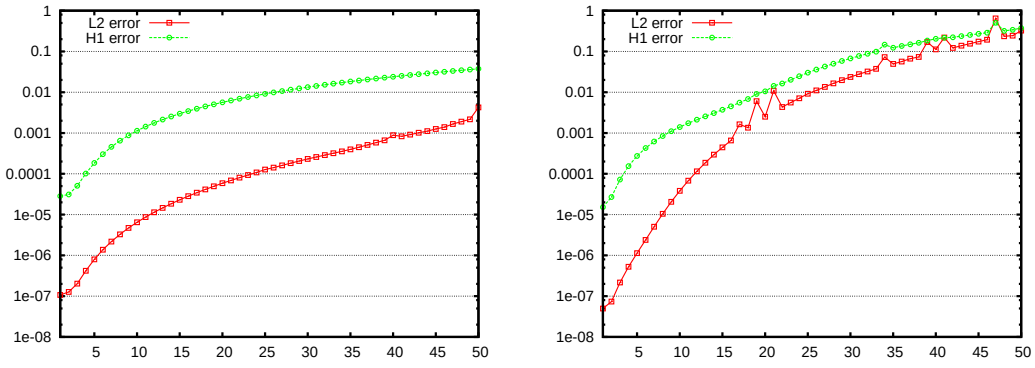

(a) $\varepsilon = 1$ (b) $\varepsilon = 10^{-20}$

Figure 5: Relative L^2 and H^1 errors between the exact solution ϕ^ε and the computed solution ϕ_M (MM) for $h = 0.0025$ (400 points in each direction) as a function of m and for $\varepsilon = 1$ respectively 10^{-20}.

and takes values (within the computational domain) in the interval $[\varepsilon_{min}, 1]$. This setting requires a novel approach to the problem since the original decomposition presented in 2.2 would yield a function q that could take values of $O(1)$ in the subdomain where ε is big and of $O(1/\varepsilon_{min})$ in the subdomain where ε is close to ε_{min}. To understand this, let us consider the simple test of Section 3.4.1, i.e. $u^\varepsilon = \sin(\pi y) + \varepsilon \cos(2\pi x) \sin(\pi y)$ with b constant and aligned with the x-axis. Let $\varepsilon = 1$ for $x < 0.5$ and $\varepsilon = \varepsilon_{min}$ for $x > 0.5$. In the decomposition $u = p + \varepsilon q$ the function p is constant in the direction of the anisotropy field b and $p|_{\Gamma_{in}} = \phi|_{\Gamma_{in}}$. In the mentioned test case $p = 2\sin(\pi y)$. For $x < 0.5$ we obtain $q = \cos(2\pi x)\sin(\pi y) - \sin(\pi y) = O(1)$. However, for $x > 0.5$ we get $q = \cos(2\pi x)\sin(\pi y) - \frac{1}{\varepsilon_{min}} \sin(\pi y) = O(1/\varepsilon_{min})$. Therefore the decomposition $u = p + \varepsilon q$ is not suitable in the case of variable ε, the function q being no more bounded.

The remedy to this deficiency is surprisingly simple. Instead of introducing the decomposition $u = p + \varepsilon q$ it suffices to define q via the following relation

$$\nabla_\parallel q = \frac{1}{\varepsilon} \nabla_\parallel u \tag{39}$$

with again $q = 0$ on Γ_{in}. This leads to almost the same system as introduced in 2.2. The only change is that the variable $\varepsilon(x)$ should be now inside the integral:

$$\begin{cases} \displaystyle\int_\Omega (A_\perp \nabla_\perp u^\varepsilon) \cdot \nabla_\perp v \, dx + \int_\Omega A_{||} \nabla_{||} q^\varepsilon \cdot \nabla_{||} v \, dx = \int_\Omega f v \, dx, & \forall v \in \mathcal{V} \\ \displaystyle\int_\Omega A_{||} \nabla_{||} u^\varepsilon \cdot \nabla_{||} w \, dx - \int_\Omega \varepsilon A_{||} \nabla_{||} q^\varepsilon \cdot \nabla_{||} w \, dx = 0, & \forall w \in \mathcal{L}\,. \end{cases} \tag{40}$$

4.1 2D test case, variable ε, uniform and aligned b-field

Let us consider a test case, where ε is close to 1 in one part of the computational domain and close to some fixed parameter ε_{min} in the remaining part. The anisotropy varies smoothly and changes its value in a relatively narrow transition region. We set

$$\varepsilon(x, y) = \frac{1}{2} \left[1 + \tanh(a(x_0 - x)) + \varepsilon_{min} (1 - \tanh(a(x_0 - x))) \right], \tag{41}$$

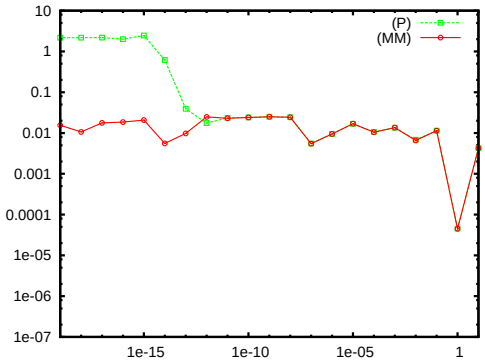

(a) L^2 error for a grid with 50×50 points.

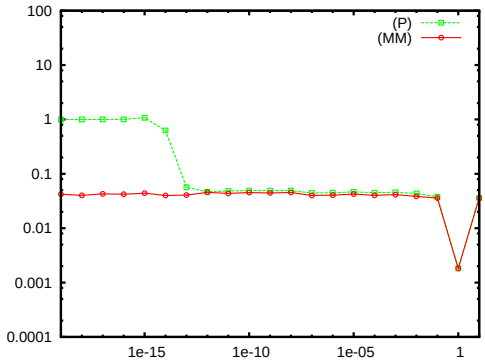

(b) H^1 error for a grid with 50×50 points.

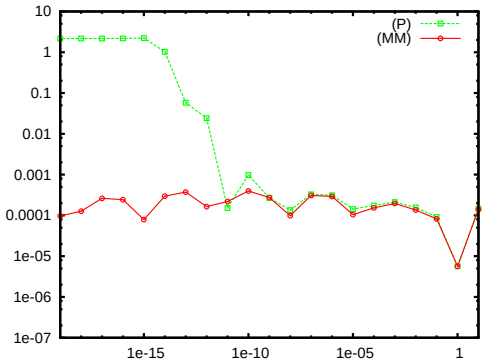

(c) L^2 error for a grid with 100×100 points.

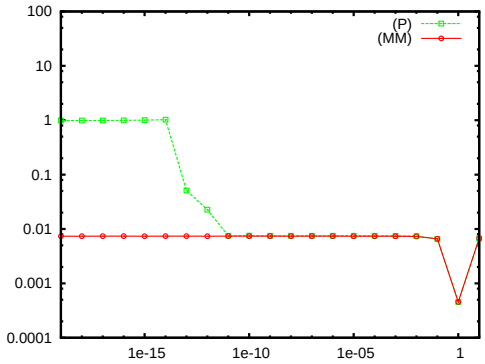

(d) H^1 error for a grid with 100×100 points.

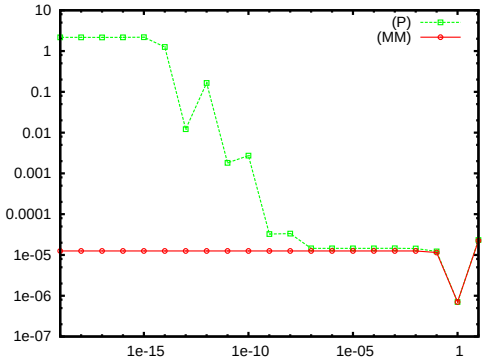

(e) L^2 error for a grid with 200×200 points.

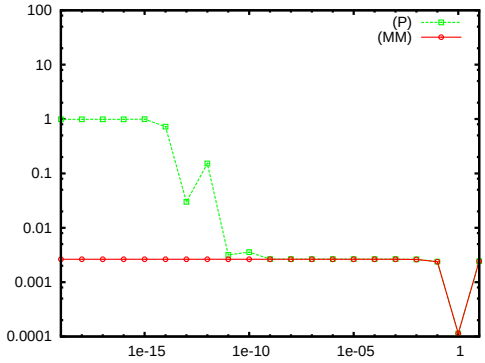

(f) H^1 error for a grid with 200×200 points.

Figure 6: Relative L^2 (left column) and H^1 (right column) errors between the exact solution u^ε and the computed numerical solution u_M (MM), u_P (P) for the test case with constant b and variable ε. The error is plotted as a function of the parameter ε_{min} and for three different mesh-sizes.

h	$\varepsilon_{min} = 1$		$\varepsilon_{min} = 10^{-20}$	
	L^2-error	H^1-error	L^2-error	H^1-error
0.1	5.7×10^{-3}	1.86×10^{-1}	2.94	9.3×10^{-1}
0.05	7.3×10^{-4}	4.7×10^{-2}	2.12×10^{-1}	7.5×10^{-1}
0.025	9.1×10^{-5}	1.18×10^{-2}	1.74×10^{-2}	1.51×10^{-1}
0.0125	1.14×10^{-5}	2.96×10^{-3}	3.14×10^{-4}	6.3×10^{-2}
0.00625	1.43×10^{-6}	7.4×10^{-4}	2.09×10^{-5}	1.29×10^{-2}
0.003125	1.78×10^{-7}	1.85×10^{-4}	2.60×10^{-6}	3.2×10^{-3}
0.0015625	2.23×10^{-8}	4.6×10^{-5}	3.3×10^{-7}	8.1×10^{-4}

Table 5: The absolute error of u in L^2 and H^1-norms for different mesh sizes and $\varepsilon_{min} = 1$ resp. $\varepsilon_{min} = 10^{-20}$ using the Micro-Macro scheme (MM) for the variable ε and constant b test case.

with a being a parameter which controls the width of the transition region and x_0 the position of the interface. In our simulations we set $x_0 = 0.25$ and $a = 50$.

Remark 8 *One should put extreme attention in coding the $\varepsilon(x, y)$ function. If ε_{min} is smaller than the numerical precision, the term $1 + \tanh(a(x_0 - x))$ dominates and hence the value of ε_{min} is never reached. Instead one should replace $1 + \tanh(a(x_0 - x))$ by the equivalent term $\frac{2e^{2a(x_0-x)}}{e^{2a(x_0-x)}+1}$, which is not limited by a computer precision.*

The solution u^ε of (4) is now given by

$$u^\varepsilon = \sin(\pi y) + \varepsilon \cos(2\pi x) \sin(\pi y)$$

and let the force term f be calculated accordingly.

As in the previous examples we solve the problem using $\mathbb{Q}_2$-FEM. We compare the results of the Micro-Macro reformulation with the Singular Perturbation model. The simulation results are presented on Figure 6. The convergence of the MM-scheme is given in the Table 5. Note that for small mesh sizes and small values of ε_{min} superconvergence occurs. This is caused by the small size of the transition region between two ε regimes. For sufficiently small meshes the convergence attains the optimal rate. Similarly as in the constant ε test cases, the Micro-Macro scheme is capable to produce the accurate results regardless of the anisotropy strength.

4.2 2D test case, variable ε, non-uniform and non-aligned b-field

In this section we choose the same test case as in Section 3.4.2 but again the epsilon varies in the computational domain and is defined by (41). The analytical solution to the problem is

$$u^\varepsilon = \sin\left(\pi y + \alpha(y^2 - y)\cos(\pi x)\right) + \varepsilon \cos(2\pi x) \sin(\pi y)$$

where $\alpha = 2$ and the force term f is calculated accordingly.

The results are shown on Figure 7. Again, contrary to the Singular Perturbation formulation, the Micro-Macro Asymptotic-Preserving formulation is capable to produce reliable numerical results regardless of the anisotropy strength. Similarly, the optimal convergence rate is attained when the mesh size is small enough to capture the ε transition.

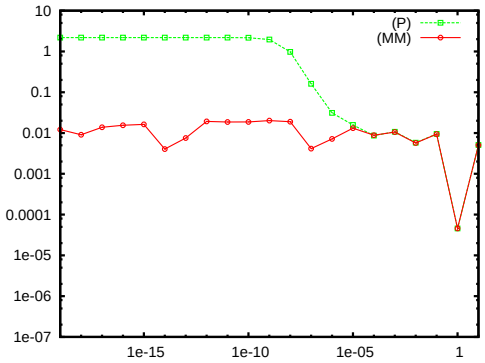

(a) L^2 error for a grid with 50×50 points.

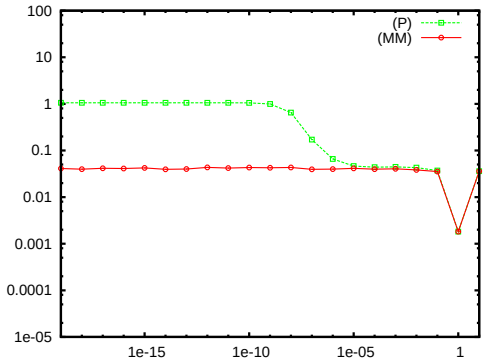

(b) H^1 error for a grid with 50×50 points.

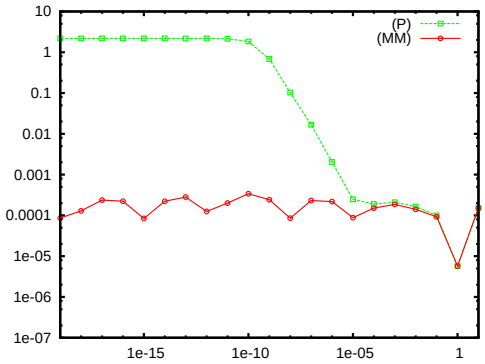

(c) L^2 error for a grid with 100×100 points.

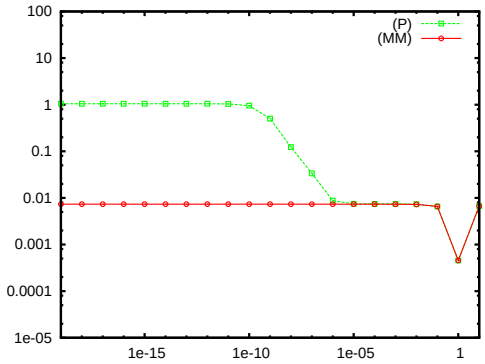

(d) H^1 error for a grid with 100×100 points.

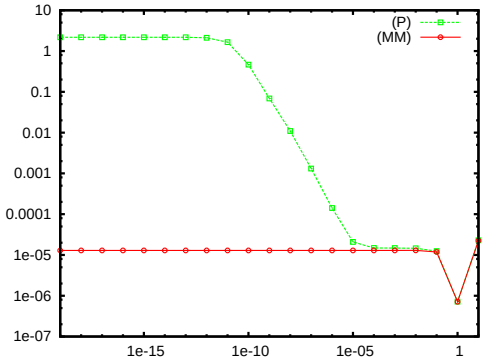

(e) L^2 error for a grid with 200×200 points.

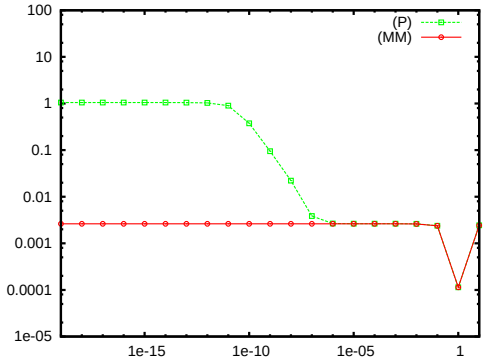

(f) H^1 error for a grid with 200×200 points.

Figure 7: Relative L^2 (left column) and H^1 (right column) errors between the exact solution u^ε and the computed numerical solution u_M (MM) resp. u_P (P) for the test case with variable b and ε. The error is plotted as a function of the parameter ε_{min} and for three different mesh-sizes.

5 Conclusion

The construction of the here introduced Micro-Macro based Asymptotic-Preserving scheme for the resolution of an anisotropic diffusion equation was based on a different reformulation of the initial Singular Perturbation problem as compared to the earlier work [6]. The advantages of the new MM-verison were shown numerically, in particular the considerable gain in simulation time and the simplicity to treat variable ε-intensities within the domain. The rigorous numerical analysis of both AP-reformulations will be the aim of a futur work, in particular the AP-property shall be shown, i.e. the uniform convergence of the scheme with respect to ε.

Acknowledgments

We acknowledge the support of the "Federation de Recherche sur la Fusion Magnétique" Euroatom and CEA, under the grand "APPLA", of the University Paul Sabatier Scientific Council under the grand "Mositer" and of the "Agence Nationale pour la Recherche (ANR)" in the frame of the contract "BOOST".

References

[1] J. Adam, J. Boeuf, N. Dubuit, M. Dudeck, L. Garrigues, D. Gresillon, A. Heron, G. Hagelaar, V. Kulaev, N. Lemoine, et al. Physics, simulation and diagnostics of Hall effect thrusters. *Plasma Physics and Controlled Fusion*, 50:124041, 2008.

[2] P. R. Amestoy, I. S. Duff, J.-Y. L'Excellent, and J. Koster. A fully asynchronous multifrontal solver using distributed dynamic scheduling. *SIAM J. Matrix Anal. Appl.*, 23(1):15–41, 2001.

[3] S. F. Ashby, W. J. Bosl, R. D. Falgout, S. G. Smith, A. F. Tompson, and T. J. Williams. A Numerical Simulation of Groundwater Flow and Contaminant Transport on the CRAY T3D and C90 Supercomputers. *International Journal of High Performance Computing Applications*, 13(1):80–93, 1999.

[4] M. Beer, S. Cowley, and G. Hammett. Field-aligned coordinates for nonlinear simulations of tokamak turbulence. *Physics of Plasmas*, 2(7):2687, 1995.

[5] C. Besse, F. Deluzet, C. Negulescu, and C. Yang. Three dimensional simulation of ionsphoric plasma disturbences. in preparation.

[6] P. Degond, F. Deluzet, A. Lozinski, J. Narski, and C. Negulescu. Duality-based asymptotic-preserving method for highly anisotropic diffusion equations. arXiv:1008.3405v1, 2010.

[7] P. Degond, F. Deluzet, L. Navoret, A.-B. Sun, and M.-H. Vignal. Asymptotic-preserving particle-in-cell method for the vlasov-poisson system near quasineutrality. *J. Comput. Phys.*, 229(16):5630–5652, 2010.

[8] P. Degond, F. Deluzet, and C. Negulescu. An asymptotic preserving scheme for strongly anisotropic elliptic problems. *Multiscale Model. Simul.*, 8(2):645–666, 2009/10.

[9] P. Degond, F. Deluzet, A. Sangam, and M.-H. Vignal. An asymptotic preserving scheme for the Euler equations in a strong magnetic field. *J. Comput. Phys.*, 228(10):3540–3558, 2009.

[10] T. Y. Hou and X.-H. Wu. A multiscale finite element method for elliptic problems in composite materials and porous media. *J. Comput. Phys.*, 134(1):169–189, 1997.

[11] S. Jin. Efficient asymptotic-preserving (AP) schemes for some multiscale kinetic equations. *SIAM J. Sci. Comput.*, 21(2):441–454, 1999.

[12] M. Kelley, W. Swartz, and J. Makela. Mid-latitude ionospheric fluctuation spectra due to secondary EŨB instabilities. *Journal of Atmospheric and Solar-Terrestrial Physics*, 66(17):1559–1565, 2004.

[13] M. Keskinen, S. Ossakow, and B. Fejer. Three-dimensional nonlinear evolution of equatorial ionospheric spread-F bubbles. *Geophys. Res. Lett*, 30(16):4–1–4–4, 2003.

[14] T. Manku and A. Nathan. Electrical properties of silicon under nonuniform stress. *Journal of Applied Physics*, 74(3):1832–1837, 1993.